

Article

A Fractional Diffusion Model for Dye-Sensitized Solar Cells

B. Maldon ^{*,†,‡}  and N. Thamwattana [‡] 

School of Mathematical and Physical Sciences, University of Newcastle, Callaghan, NSW 2308, Australia; natalie.thamwattana@newcastle.edu.au

* Correspondence: benjamin.maldon@uon.edu.au

† Current address: University Drive, Callaghan, NSW 2308, Australia.

‡ These authors contributed equally to this work.

Received: 8 June 2020; Accepted: 27 June 2020; Published: 28 June 2020



Abstract: Dye-sensitized solar cells have continued to receive much attention since their introduction by O'Regan and Grätzel in 1991. Modelling charge transfer during the sensitization process is one of several active research areas for the development of dye-sensitized solar cells in order to control and improve their performance and efficiency. Mathematical models for transport of electron density inside nanoporous semiconductors based on diffusion equations have been shown to give good agreement with results observed experimentally. However, the process of charge transfer in dye-sensitized solar cells is complicated and many issues are in need of further investigation, such as the effect of the porous structure of the semiconductor and the recombination of electrons at the interfaces between the semiconductor and electrolyte couple. This paper proposes a new model for electron transport inside the conduction band of a dye-sensitized solar cell comprising of TiO₂ as its nanoporous semiconductor. This model is based on fractional diffusion equations, taking into consideration the random walk network of TiO₂. Finally, the paper presents numerical solutions of the fractional diffusion model to demonstrate the effect of the fractal geometry of TiO₂ on the fundamental performance parameters of dye-sensitized solar cells, such as the short-circuit current density, open-circuit voltage and efficiency.

Keywords: dye-sensitized solar cells; electron density; fractional diffusion; subdiffusion; titanium dioxide; mathematical modelling

1. Introduction

Dye-sensitized solar cells (DSSCs) were first introduced by O'Regan and Grätzel in their fundamental 1991 paper [1], providing a viable low-cost alternative for renewable solar energy. Functionally, DSSCs operate by a photosensitive dye using absorbed sunlight to inject excited electrons into a nanoporous semiconductor. This approach relieves DSSCs of the need for a costly and high purity semiconductor as opposed to the predominant silicon solar cells that have been at the forefront of solar energy since 1954 [2].

Mathematical modelling for DSSCs began shortly afterwards and continues to offer unique insight into the current–voltage relationship and ultimately the efficiency of the DSSC. While some early mathematical models of DSSCs used Maxwell's equations and electric potentials [3], Gregg [4] outlined the prevalence of the photoinduced potential as more influential than electric fields in DSSCs. Södergren et al. [5] were the first to model DSSCs by a simple diffusion equation together with analytical expressions for the short-circuit current density J_{sc} and the open-circuit

voltage V_{oc} . Cao et al. [6] extended the model to include time-dependence, leading to the partial differential equation

$$\frac{\partial n}{\partial t} = D_0 \frac{\partial^2 n}{\partial x^2} + \varphi \alpha e^{-\alpha x} - k_R (n(x, t) - n_{eq}), \quad (1)$$

where $n(x, t)$ is the conduction band electron density at depth $x \in [0, d]$ and time $t \geq 0$, D_0 is the diffusion coefficient, φ is the incident photon flux, α is the absorption coefficient, k_R is the recombination constant and n_{eq} is the equilibrium electron density.

Anta et al. [7] considered a fully nonlinear diffusion equation for DSSCs and investigated the effect of different power-law diffusivities, which was analysed using Lie symmetry by Maldon et al. 2020 [8]. Andrade et al. 2011 [9] and Gacemi et al. 2013 [10] proposed diffusion equations for modelling the electrolyte concentrations, which were solved analytically by Maldon and Thamwattana in 2019 [11].

Fractional calculus has existed conceptually as long as calculus itself. For close to three centuries, fractional calculus had only one known application in Abel's 1823 tautochrone problem [12] until Nigmatullin [13] suggested a fractional diffusion equation for modelling media exhibiting a fractal geometry. In 2000, Henry and Wearne [14] developed the standard fractional diffusion equation based on continuous-time random-walk (CTRW) models. Henry and Wearne's model [14], together with the CTRW simulation of TiO_2 by Nelson [15], provides motivation for this paper to model DSSCs using fractional partial differential equations.

Modelling DSSCs with fractional calculus is a relatively unexplored research direction. So far, there is only one paper by Sibatov et al. in 2014 [16]. In Sibatov et al. [16], they consider the role of trap states within the TiO_2 network and its effect on the electron hole density. To address the fact that previous mathematical models for DSSCs do not generally consider the effect of the porous network in TiO_2 [6,17], we develop our model based on generalised fractional diffusion-reaction equations, taking this effect into account.

For this study, we use the Caputo fractional derivative, which is given by [18]

$$\frac{d^\lambda f}{dt^\lambda} = \begin{cases} f^{(\lambda)}(t), & \text{if } \lambda \in \mathbb{N}, \\ \int_0^t \frac{(t-\tau)^{(n-\lambda-1)}}{\Gamma(n-\lambda)} f^{(n)}(\tau) d\tau, & \end{cases} \quad (2)$$

where $\lambda > 0$ is the order of the fractional derivative, $n = \lceil \lambda \rceil$, $f^{(n)}(t)$ denotes the classical derivative of f with respect to its variable of order $n \in \mathbb{N}$ and Γ is the usual Gamma function

$$\Gamma(z) = \int_0^\infty x^{z-1} e^{-x} dx.$$

The literature employs several definitions for the fractional derivative in modelling diffusion in media exhibiting a fractal geometry. Henry and Wearne [14] suggest the Riemann–Liouville definition, but also remark that the Caputo definition has also seen some use [14,19]. However, Baeumer et al. [20] comment on the use of Caputo derivatives for space-fractional diffusion models that positivity is not preserved under vanishing Neumann boundary conditions. We find that problem is alleviated by the use of a time-fractional derivative on the diffusion term of our equation. Also, the presence of spatially dependent source terms and the combination of Dirichlet and Neumann boundary conditions enjoy a greater level of compatibility with the Caputo fractional derivative [21].

2. Mathematical Model

In this paper, we adopt a Caputo fractional derivative in time on the diffusion term as shown by Henry and Wearne [14], resulting in the fractional partial differential equation (FPDE)

$$\frac{\partial n}{\partial t} = D_0 \frac{\partial^{1-\gamma}}{\partial t^{1-\gamma}} \left(\frac{\partial^2 n}{\partial x^2} \right) + \varphi \alpha e^{-\alpha x} - k_R (n(x, t) - n_{eq}), \quad (3)$$

where $\gamma \in (0, 1]$ is the order of the Caputo fractional derivative in time and all other parameters retain their values as in Equation (1). Physically, the parameter γ is the exponent in the mean square displacement of the CTRW simulation [14]. The special case $\gamma = 1$ recovers the standard diffusion equation. Lower values for γ correspond to longer path lengths for electron transport through the nanoporous semiconductor [22]. The parameter γ is also strongly influenced by the porosity of the TiO₂ semiconductor. Benkstein et al. [22] found that increasing porosity led to a decrease in γ . We note that Equation (3) does not feature the term

$$D_0 \mathcal{L}^{-1} \left(\frac{\partial^{-\gamma}}{\partial t^{-\gamma}} \frac{\partial^2 n}{\partial x^2} \Big|_{t=0} \right),$$

where \mathcal{L}^{-1} denotes the inverse Laplace transformation. Though this term is critical for physically meaningful fractional diffusion equations [14], it vanishes in Equation (3) under the Caputo fractional derivative.

We prescribe boundary conditions as found in [5], with a Dirichlet boundary condition at $x = 0$ and a Neumann boundary condition at $x = d$ together with a prescribed initial condition, namely

$$n(0, t) = n_{eq} e^{\frac{qV}{mk_B T}}, \quad (4)$$

$$\frac{\partial n}{\partial x} \Big|_{x=d} = 0, \quad (5)$$

$$n(x, 0) = n_{eq} e^{\frac{qV}{mk_B T}}, \quad (6)$$

where q is the standard electron charge, V is the bias voltage, m is the diode ideality factor, k_B is Boltzmann's constant and T is the temperature of the DSSC.

The diode equation is commonly used to compute the current–density relationship for solar cells, in which the current J as a function of bias voltage V is given by

$$J(V) = J_{sc} - J_0 \left(e^{\frac{qV}{mk_B T}} - 1 \right), \quad (7)$$

where J_0 is the dark saturation current density, given by Södergren et al. [5] in the form

$$J_0 = qn_{eq} \sqrt{D_0 k_R} \tanh \left(\sqrt{\frac{k_R}{D_0}} d \right).$$

To compute the short-circuit current density J_{sc} we use

$$J_{sc} = qD_0 \left[\frac{\partial^{1-\gamma}}{\partial t^{1-\gamma}} \left(\frac{\partial n}{\partial x} \right) \right] \Big|_{x=0}, \quad (8)$$

noting that the standard flux is recovered in the special case of linear diffusion ($\gamma = 1$).

Given that the open-circuit voltage V_{oc} satisfies $J(V_{oc}) = 0$, we may compute the open-circuit voltage from

$$V_{oc} = \frac{mk_B T}{q} \ln \left(\frac{J_{sc}}{J_0} + 1 \right).$$

Maximising the power output $P(V) = VJ(V)$ over V , we obtain the maximum power point V_{max} by

$$V_{max} = \frac{mk_B T}{q} \left(W \left(e^{\frac{J_{sc} + J_0}{J_0}} \right) - 1 \right),$$

where W is the Lambert-W function and $J_{max} = J(V_{max})$. With $P_{max} = V_{max}J_{max}$, we compute the efficiency η of the DSSC by

$$\eta = \frac{P_{max}}{P_i},$$

where P_i is the power of incident light.

3. Finite Difference Method

Finite difference methods (FDMs) have been used by Hu et al. [23] to solve parabolic FPDEs under the Caputo fractional derivative for fractional time derivatives, and Takeuchi et al. [24] have used finite difference methods to solve FPDEs under fractional spatial derivatives. We refer the reader to Li and Zeng [25] for a finite difference scheme for solving fractional ordinary differential equations over a finite interval under boundary conditions defined at the left boundary.

In this paper, we solve Equation (3) under a FDM scheme using expressions given by Oldham and Spanier [26]. All numerical computations are performed using numerical values of constants provided in Table 1 except for γ , which is given several values in Table 2.

Table 1. Parameter values for the Dye-Sensitized Solar Cell (DSSC) model.

Parameter	Value	Unit	Reference
D_0	10^{-11}	m^2s^{-1}	[7]
α	10^5	m^{-1}	[10]
d	5×10^{-5}	m	[7]
k_R	4×10^{-8}	s^{-1}	[7]
m	1	-	[5]
n_{eq}	10^{22}	m^{-3}	[27]
P_i	10	Wm^{-2}	[10]
φ	10^{21}	$m^{-2}s^{-1}$	[28]

To numerically solve Equation (3) under boundary conditions (4)–(6) with a finite difference scheme, we use the L1 approximation for the fractional derivative given by Oldham and Spanier [26] in which

$$\left. \frac{\partial^\gamma f}{\partial t^\gamma} \right|_{t=t_n} \approx \frac{(\Delta t)^{-\gamma}}{\Gamma(2-\gamma)} \sum_{k=0}^{n-1} b_k^\gamma [f(t_{n-k}) - f(t_{n-k-1})], \tag{9}$$

where b_k^γ is given by

$$b_k^\gamma = (k+1)^{1-\gamma} - k^{1-\gamma}.$$

Let $t_f > 0$ be the final simulation time. Discretise $[0, t_f]$ into N_t nodes and $[0, d]$ into $N_x + 1$ nodes, and let $u_{i,j}$ estimate the solution to Equation (3) under the boundary conditions (4)–(6) at the point $((j-1)\Delta x, (i-1)\Delta t)$. That is,

$$n((j-1)\Delta x, (i-1)\Delta t) \approx u_{i,j}. \tag{10}$$

3.1. Nodes Determined by Boundary Conditions

To satisfy the initial condition (6), we set

$$u_{1,j} = n_{eq} e^{\frac{qV}{mk_B T}},$$

for all $j \in \{1, \dots, N_x + 1\}$. For the boundary condition (4) at $x = 0$, we set

$$u_{i,1} = n_{eq} e^{\frac{qV}{mk_B T}},$$

for all $i \in \{1, \dots, N_t\}$. Finally, for the Neumann boundary condition (5) at $x = d$ we employ a ‘ghost node’ at $x = d + \Delta x$ and a central difference approximation for the first derivative at $x = d$ to set

$$u_{i,Nx+1} = u_{i,Nx-1},$$

for all $i \in \{1, \dots, N_t\}$.

3.2. Iteration Algorithm

For the second row $i = 2$, we have

$$\begin{aligned} u_{2,j} &= u_{1,j} + (\Delta t)\varphi\alpha e^{-\alpha(j-1)(\Delta x)} - k_R(u_{1,j} - n_{eq}) \\ &= n_{eq} + (\Delta t)\varphi\alpha e^{-\alpha(j-1)(\Delta x)}. \end{aligned}$$

Given $i \in \{2, \dots, N_t\}$ and $j \in \{2, \dots, Nx\}$, the finite difference iteration for numerically solving Equation (3) is given by

$$\begin{aligned} u_{i+1,j} &= u_{i,j} + D_0 \frac{(\Delta t)^\gamma}{\Gamma(\gamma + 1)} \sum_{k=0}^{i-2} [(k+1)^\gamma - k^\gamma] \times \\ &\left(\frac{u_{i-k,j+1} - 2u_{i-k,j} + u_{i-k,j-1} - u_{i-k-1,j+1} + 2u_{i-k-1,j} - u_{i-k-1,j-1}}{(\Delta x)^2} \right) \\ &+ (\Delta t) \left[\varphi\alpha e^{-\alpha(j-1)(\Delta x)} - k_R(u_{i,j} - n_{eq}) \right]. \end{aligned} \quad (11)$$

3.3. Estimate for Short-Circuit Current Density

To compute the short-circuit current density, we must estimate the electron flux at $x = 0$. We achieve this by a 10 point estimate of the form

$$\begin{aligned} \left. \frac{\partial n}{\partial x} \right|_{x=0} &\approx a_0 n(0) + a_1 n(\Delta x) + a_2 n(2\Delta x) + a_3 n(3\Delta x) + a_4 n(4\Delta x) \\ &+ a_5 n(5\Delta x) + a_6 n(6\Delta x) + a_7 n(7\Delta x) + a_8 n(8\Delta x) + a_9 n(9\Delta x), \end{aligned} \quad (12)$$

where a_i is a constant for each $i = 0, 1, \dots, 9$. We determine these constants so that polynomials are perfectly estimated up to degree 9. This leads to the constants

$$\begin{aligned} a_0 &= -\frac{7129}{2520(\Delta x)}, a_1 = \frac{9}{(\Delta x)}, a_2 = -\frac{18}{(\Delta x)}, a_3 = \frac{28}{(\Delta x)}, a_4 = -\frac{63}{2(\Delta x)}, \\ a_5 &= \frac{126}{5(\Delta x)}, a_6 = -\frac{14}{(\Delta x)}, a_7 = \frac{36}{7(\Delta x)}, a_8 = -\frac{9}{8(\Delta x)}, a_9 = \frac{1}{9(\Delta x)}. \end{aligned}$$

4. Results and Discussion

Using the finite difference method, we numerically solve Equation (3) for several values of γ using 10 spatial nodes and 5000 temporal nodes over $x \in [0, d]$ and $t = 100$ s. To investigate the effect of the parameter γ , we plot numerical solutions for the special cases $\gamma = 0.25, 0.5, 0.75$ and 1 in Figure 1.

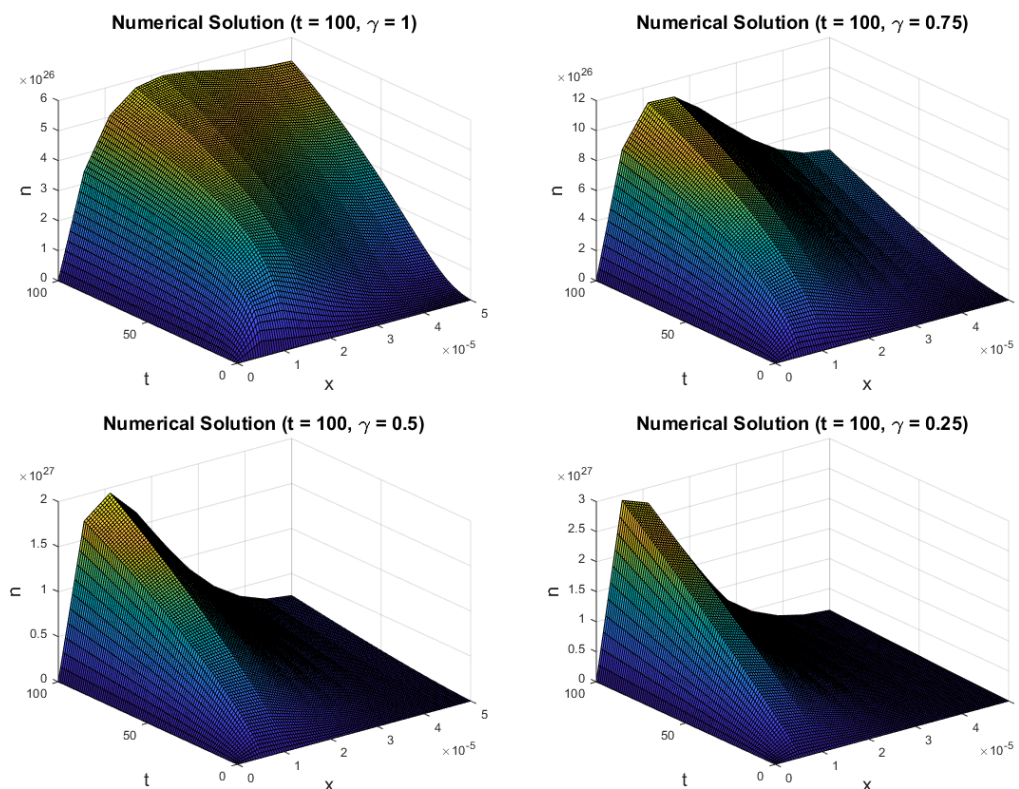


Figure 1. Plots of the numerical solution to Equation (3) against x and t for $\gamma = 1$ (top-left), $\gamma = 0.75$ (top-right), $\gamma = 0.5$ (bottom-left), $\gamma = 0.25$ (bottom-right).

Using the numerical solutions to Equation (3) and the flux estimate given by Equation (12), we are able to compute the short-circuit current density J_{sc} and the open-circuit voltage V_{oc} , leading to the overall efficiency η . Table 2 shows the effect of the parameter γ on these DSSC performance parameters.

Table 2. Values for J_{sc} , V_{oc} and η for several values of γ at time $t = 100$ s.

γ	J_{sc} (Am^{-2})	V_{oc} (V)	η (%)
0.25	56.0248	0.6056	2.8144
0.39	70.7900	0.6117	3.5967
0.5	82.6370	0.6156	4.23
0.612	94.6085	0.6191	4.8741
0.75	108.9019	0.6227	5.6481
1	134.2799	0.6281	7.03

From Table 2, we see that the short-circuit current density J_{sc} increases when γ increases. Though the open-circuit voltage is not affected to the same extent, the efficiency is notably lower for decreased values of γ . We note the special case $\gamma = 1$ is equivalent to the standard diffusion equation without fractional derivatives, and the efficiency $\eta = 7.03\%$ is in agreement with expected efficiencies for DSSCs [8].

As γ decreases, Figure 1 presents two primary trends to the numerical solution to Equation (3). Firstly, the time required to reach steady-state increases as γ decreases by comparison to the numerical solutions for the cases $\gamma = 1$ and 0.25. This result is consistent with the observation that lower values for γ imply slower diffusion, based on the CTRW simulations. Benkstein et al. [22] show that γ decreases when porosity increases from $p = 0.7$ to $p = 0.775$.

Secondly, the overall electron density is remarkably higher for the cases $\gamma = 0.5$ and 0.25 compared to $\gamma = 1$ and 0.75. This suggests that the electron density is highly sensitive to the order

of the fractional derivative. The standard gradient for flux would consequently produce extreme results, requiring the fractional derivative to rectify this issue. Numerically, the finite difference scheme presents stability problems and is computationally expensive for lower values of γ .

The parameter γ denotes the exponent for the power-law in the mean-square displacement [14]. We conclude from Figure 1 that lower values of γ lead to progressively less realistic behaviour for nanoporous semiconductors used in DSSCs, as the electron density dramatically increases when γ decreases. This observation is consistent with the longer path lengths associated with low values for γ in CTRW simulation. In particular, Ni et al. [27] show that extremely low porosities (such as $p = 0.1$) show a significant reduction in efficiency (below 1%). From the numerical solution to Equation (3) with $\gamma = 0.612$ using 25 spatial nodes, the flux estimate given by Equation (12) and 50,000 temporal nodes to $t = 500$ s, we find $J_{sc} = 116.9059 \text{ Am}^{-2}$, $V_{oc} = 0.6245 \text{ V}$ and $\eta = 6.0835\%$.

5. Conclusions

We propose a new mathematical model for evaluating the efficiency of dye-sensitized solar cells by using fractional diffusion to incorporate the fractal geometry of the TiO_2 semiconductor. Our results show that lower values of the mean square exponent γ lead to lower efficiencies, a result that is consistent with the literature [11,27]. In particular, figure 11 of Ni et al. [27] shows that efficiency decreases when porosity increases above $p = 0.4$ or decreases below $p = 0.4$, which suggests the relationship between porosity and efficiency is nonlinear. We note that the solution profile of the electron density presented here is similar to those obtained from nonlinear diffusion modelling [8], though the orders of magnitude differ significantly. This is due to the longer waiting times associated with lower values for γ , which slows down the diffusion process.

We also develop a finite difference scheme to numerically solve the fractional diffusion equation and provided a tenth-order estimate for obtaining the short-circuit current density. Together, this provides a comprehensive model for incorporating the effect of the random-walk behaviour of the nanoporous semiconductor on the performance of dye-sensitized solar cells.

Future consideration includes incorporating the role of the electrolyte couple by a pair of standard diffusion equations as seen in Maldon and Thamwattana [11].

Author Contributions: Conceptualization, B.M. and N.T.; methodology, B.M. and N.T.; software, B.M.; validation, B.M.; formal analysis, B.M.; investigation, B.M.; resources, B.M.; data curation, B.M.; writing—original draft preparation, B.M.; writing—review and editing, N.T.; visualization, B.M.; supervision, N.T.; project administration, N.T.; funding acquisition, N. Thamwattana. All authors have read and agreed to the published version of the manuscript.

Funding: This research was funded by the Australian Research Council Discovery Project DP170102705.

Acknowledgments: This research has been conducted with the support of the Australian Government Research Training Program Scholarship.

Conflicts of Interest: The authors declare no conflict of interest.

Abbreviations

The following abbreviations are used in this manuscript:

DSSC	Dye-Sensitized Solar Cell
FPDE	Fractional Partial Differential Equation
TiO_2	Titanium Dioxide

References

1. O'Regan, B.; Grätzel, M. A low-cost, high-efficiency solar cell based on dye-sensitized colloidal TiO_2 films. *Nature* **1991**, *353*, 737–740. [[CrossRef](#)]
2. Chapin, D.L.; Fuller, C.S.; Pearson, G.L. A new Silicon junction photocell for converting solar radiation into electrical power. *J. Appl. Phys.* **1954**, *25*, 676–677. [[CrossRef](#)]

3. Ferber, J.; Stangl, R.; Luther, J. An electrical model of the dye-sensitized solar cell. *Sol. Energy Mater. Sol. Cells* **1998**, *53*, 29–54. [[CrossRef](#)]
4. Gregg, B.A. Comment on “Diffusion impedance and space charge capacitance in the nanoporous dye-sensitized electrochemical solar cell” and “Electronic transport in dye-sensitized nanoporous TiO₂ solar cells—Comparison of electrolyte and solid-state devices”. *J. Phys. Chem. B* **2003**, *107*, 13540. [[CrossRef](#)]
5. Södergren, S.; Hagfeldt, A.; Olsson, J.; Lindquist, S. Theoretical Models for the Action Spectrum and the Current-Voltage Characteristics of Microporous Semiconductor Films in Photoelectrochemical Cells. *J. Phys. Chem.* **1994**, *98*, 5552–5556. [[CrossRef](#)]
6. Cao, F.; Oskam, G.; Meyer, G.J.; Searson, P.C. Electron Transport in Porous Nanocrystalline TiO₂ Photoelectrochemical Cells. *J. Phys. Chem.* **1996**, *100*, 17021–17027. [[CrossRef](#)]
7. Anta, J.A.; Casanueva, F.; Oskam, G. A numerical model for charge transport and recombination in dye-sensitized solar cells. *J. Phys. Chem. B* **2006**, *110*, 5372–5378. [[CrossRef](#)]
8. Maldon, B.; Thamwattana, N.; Edwards, M. Exploring nonlinear diffusion equations for modelling dye-sensitized solar cells. *Entropy* **2020**, *22*, 248. [[CrossRef](#)]
9. Andrade, L.; Sousa, J.; Ribeiro, H.A.; Mendes, A. Phenomenological modeling of dye-sensitized solar cells under transient conditions. *Sol. Energy* **2020**, *85*, 781–793. [[CrossRef](#)]
10. Gacemi, Y.; Cheknane, A.; Hilal, H.S. Simulation and modelling of charge transport in dye-sensitized solar cells based on carbon nano-tube electrodes. *Phys. Scr.* **2013**, *87*, 035703–035714. [[CrossRef](#)]
11. Maldon, B.; Thamwattana, N. An analytical solution for charge carrier densities in dye-sensitized solar cells. *J. Photoch. Photobiol. A* **2019**, *370*, 41–60. [[CrossRef](#)]
12. Herrmann, R. *Fractional Calculus: An Introduction for Physicists*; World Scientific Publishing Co. Pty. Ltd.: Singapore, 2014.
13. Nigmatullin, R. The realization of the generalised transfer equation in a medium with fractal geometry. *Phys. Status Solidi B* **1986**, *133*, 425–430. [[CrossRef](#)]
14. Henry, B.I.; Wearne, S.L. Fractional reaction-diffusion. *Phys. A* **2000**, *276*, 448–455. [[CrossRef](#)]
15. Nelson, J. Continuous-Time Random-Walk Model of Electron Transport in Nanocrystalline TiO₂ Electrodes. *Phys. Rev. B* **1999**, *59*, 15374–15380. [[CrossRef](#)]
16. Sibatov, R.T.; Svetukhin, V.V.; Uchaikin, V.V.; Morozova, E.V. Fractional Model of Electron Diffusion in Dye-Sensitized Nanocrystalline Solar Cells. In International Conference on Mathematical Models and Methods in Applied Sciences, Saint Petersburg, Russia, 23–25 September 2014; pp. 118–121.
17. Koster, L.J.A.; Smits, E.C.P.; Mihailetschi, V.D.; Blom, P.W.M. Device model for the operation of polymer/fullerene bulk heterojunction solar cells. *Phys. Rev. B* **2005**, *72*, 085205.1–085205.9. [[CrossRef](#)]
18. Duan, J. S.; Fu, S. Z.; Wang, Z. Fractional diffusion-wave equations on finite interval by Laplace transform. *Integral Transform. Spec. Funct.* **2014**, *25*, 220–229. [[CrossRef](#)]
19. Caputo, M. Linear models of dissipation whose Q is almost frequency independent—II. *Geophys. J. Int.* **1967**, *13*, 529–539. [[CrossRef](#)]
20. Baeumer, B.; Kovács, M.; Meerschaert, M.; Sankaranarayanan, H. Reprint of: Boundary conditions for fractional diffusion. *J. Comput. Appl. Math.* **2018**, *339*, 414–430. [[CrossRef](#)]
21. Garrappa, R.; Kaslik, E.; Papolizio, M. Evaluation of fractional integrals and derivatives of elementary functions: Overview and tutorial. *Mathematics* **2019**, *7*, 407–428. [[CrossRef](#)]
22. Benkstein, K.D.; Kopidakis, N.; van de Lagemaat, J.; Frank, A.J. Influence of the percolation network geometry on electron transport in dye-sensitized titanium dioxide solar cells. *J. Phys. Chem. B* **2003**, *107*, 7759–7767. [[CrossRef](#)]
23. Hu, Y.; Li, C.; Li, H. The finite difference method for Caputo-type parabolic equation with fractional Laplacian: One dimension case *Chaos Soliton. Fract.* **2017**, *102*, 319–326. [[CrossRef](#)]
24. Takeuchi, Y.; Yoshimoto, Y.; Suda, R. Second order accuracy finite difference methods for space-fractional partial differential equations. *J. Comput. Appl. Math.* **2017**, *320*, 101–109. [[CrossRef](#)]
25. Li, C.; Zeng, F. The finite difference methods for fractional ordinary differential equations. *Numer. Funct. Anal. Opt.* **2013**, *34*, 149–179. [[CrossRef](#)]
26. Oldham, K.; Spanier, J. *The Fractional Calculus: Theory and Applications of Differentiation and Integration of Arbitrary Order*; Academic Press: San Diego, CA, USA, 1974.

27. Ni, M.; Leung, M.K.H.; Leung, D.Y.C.; Sumathy, K. An analytical study of the porosity effect on dye-sensitized solar cell performance. *Sol. Energy Mater. Sol. Cells* **2006**, *90*, 1331–1344. [[CrossRef](#)]
28. Gómez, R.; Salvador, P. Photovoltage Dependence on Film Thickness and Type of Illumination in Nanoporous Thin Film Electrodes According to a Simple Diffusion Model. *Sol. Energy Mater. Sol. Cells* **2005**, *88*, 377–388. [[CrossRef](#)]



© 2020 by the authors. Licensee MDPI, Basel, Switzerland. This article is an open access article distributed under the terms and conditions of the Creative Commons Attribution (CC BY) license (<http://creativecommons.org/licenses/by/4.0/>).